Fundamental Approach to the Design and Optimization of Static Mixers

E. S. Szalai and F. J. Muzzio
Dept. of Chemical and Biochemical Engineering, Rutgers University, Piscataway, NJ 08854

Mixing in the Kenics static mixer is optimized using computational analysis and theoretical concepts. A total of 54 cases were examined to consider the effect of mixer geometry and inertia on flow and mixing performance. The effect of varying the standard geometry is discussed for a broad range of Reynolds numbers. While only the twist angle affects performance at low flow rates ($Re \cong 1$), both the element aspect ratio and the twist angle are shown to be important at high flow rates ($Re \leq 1{,}000$). The energetic mixing efficiency decreases with increasing flow rate. Finally, a quality-driven design method is developed based on stretching calculations, and is illustrated for the standard mixer design.

Introduction

While substantial progress has been achieved in recent years in understanding laminar mixing processes, *a priori* methods for designing mixing processes under practical conditions are still unavailable. Most prior work falls into two main categories: in-depth analyses of two-dimensional (2-D) model systems that have limited practical relevance, or forensic (*a posteriori*) descriptions of realistic systems that provide useful information about the case at hand, but that are difficult to generalize to other situations.

In this article, we use recently developed fundamental concepts from dynamical systems theory to predict and optimize mixing performance under a wide range of realistic design and operating conditions. We use the Kenics static mixer, which is one of the simplest and most common industrial mixers (more than 10 million disposable units are sold annually for many different applications), in combination with a highly accurate CFD approach, to characterize the evolution of the mixing process, and to develop rational methods for designing and optimizing mixing performance.

Static mixers consist of a series of flow reorientation devices inserted along the axis of a pipe. Pressure (as opposed to mechanical agitation) drives the fluid through the device, providing the energy needed to accomplish mixing. Static mixers are often used to disperse immiscible fluids (Taweel and Chen, 1996), or to promote heat and mass transfer in viscous fluids (Grace 1971; Morris and Benyon, 1976; van der Meer and Hoogedoorn, 1978; Wang and Fan, 1978; Naumann, 1979; Ishikawa and Kamiya, 1994; Lang et al., 1995; Chisti and Moo-Young, 1996; Li et al., 1996; Del Carmen Rey et al., 1998; Cavatorta and Bohm, 1999).

Numerous designs are on the market for static mixers. The most common geometries include the SMX and the Kenics static mixers. Experimental investigations of static mixers have measured pressure drops, residence time distributions, and power consumption (Nigam and Naumann, 1985; Pustelnik, 1986; Kemblowski and Pustelnik, 1988; Naumann, 1991). Flow visualization in these devices is difficult due to their complex geometry, although mixing patterns at the discharge of the mixer has been accomplished (Jaffer and Wood, 1998). Due to a dearth of rigorous design information, equipment design and scale-up in the laminar and transitional regimes for static mixers is difficult. Some correlation methods are available for a limited range of operating conditions and applications. However, process equipment design is often based on past experience and/or trial-error procedures.

Computational fluid dynamics (CFD) is an increasingly effective alternative to speed up equipment design and gain additional fundamental understanding of mixing processes. Only a few detailed computational studies of static mixers have been performed to date. In earlier studies, the effects of flow rate and geometry on Kenics mixing performance were separately considered (Bakker, 1993; Ling and Zhang, 1995; Avalosse and Crochet, 1997; Hobbs et al., 1997; Rauline et al., 1998, 2000).

Correspondence concerning this article should be addressed to F. J. Muzzio.

While none of these studies examined in detail the mechanisms that controlled mixture pattern evolution, they provide a firm basis for the work presented here. The remainder of this article is organized as follows: the system under investigation is described and the numerical methods are used to examine flow and mixing processes. The mixing performance of the standard Kenics mixer is analyzed. The effect of nonstandard geometries is considered. The main result presented in this section is that operational and energetic performance depend nonmonotonically on geometry and flow rate, thus highlighting the value of effective CFD approaches capable of considering the exact case of interest, rather than correlation-based methods that necessarily rely on inter- (and extra-) polation. After basic concepts are firmly established, a quality-based approach is developed for design and optimization of mixing applications using the standard Kenics geometry followed by a summary, conclusions, and discussion of possible extensions.

System Geometry and Computational Methods

Figure 1 shows a six-element standard Kenics configuration. Each element is twisted by 180 degrees, alternating clockwise and counterclockwise twists. The elements are arranged with the trailing edge of each element perpendicular to the leading edge of the next one. In the remainder of this article, the mixer housing is assumed to be a cylindrical tube with diameter $D = 0.0508$ m, and the material thickness of each mixer element is 2 mm. L represents the length of one mixer element. This parameter is equal to 0.0508 m for the $L/D = 1$ geometry, 0.0762 m for the standard Kenics with $L/D = 1.5$, and 0.1016 m for the $L/D = 2$ case. In our simulations, an entrance and exit section of two element lengths is added to the pipe to assure well-developed flow into and out of the mixer region.

Fluid properties in the simulations were similar to glycerin at room temperature, with density equal to 1,200 kg/m^3 and viscosity at 0.5 kg/(m·s). Nine mixer geometries were considered in the present analysis and are described in Table 1. The effect on flow and mixing of two geometric parameters,

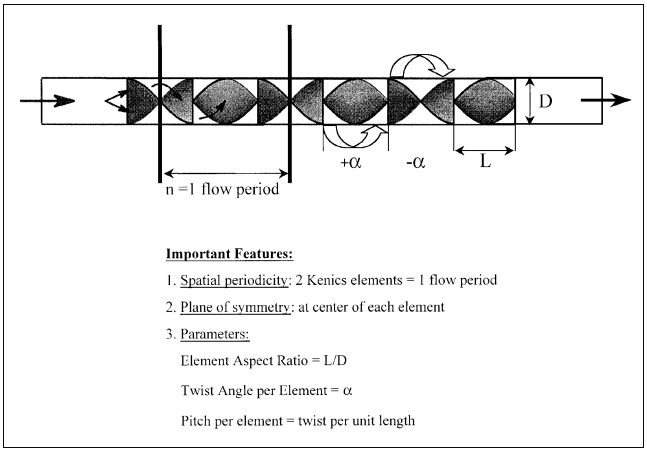

Figure 1. Geometry of a six-element Kenics static mixer.

The element length-to-diameter ratio (L/D) is 1.5 and the twist angle is 180 degrees in the standard design.

Table 1. Geometric Parameters

Geometry	Aspect Ratio (L/D)	Twist Angle per Element
1	1.0	120.0
2	1.0	150.0
3	1.0	180.0
4	1.5	120.0
5	1.5	150.0
6*	1.5	180.0
7	2.0	120.0
8	2.0	150.0
9	2.0	180.0

*Standard Kenics mixer.

the element twist angle, and L/D ratio were examined under both creeping flow and inertial conditions. While it has already been established that the L/D ratio does not affect mixing in the creeping flow Newtonian limit, different trends are evident at higher Reynolds numbers. The Reynolds number was varied from 21.5 to 1,000, and six different flow conditions spanning the transitional regime were considered in each of the 9 geometries: $Re = 10(10)^{1/3}$, $10(100)^{1/3}$, 100, $100(10)^{1/3}$, $100(100)^{1/3}$ and 1,000 (summarized in Table 2.) Thus, a total of 54 flows were computed and analyzed in this study.

The computational methods used to simulate flow and mixing processes have been previously validated for a variety of systems, so only a brief summary is included here; for details, see Zalc et al. (1999, 2001). An unstructured mesh made of first-order, four-node tetrahedral elements was constructed for each geometry using a geometry builder and mesh generator software (ICEM CFD, Berkeley, CA). The average element aspect ratio was 2.2. The mixer geometry was discretized to a total of about 3 million elements using 700,000 nodes. The solutions for each velocity field required about 2 CPU h and 1.2 Gbytes of memory on a single processor using Acusolve (Acusim Inc., Sarratoga, CA). In order to avoid discontinuities in the numerical solution the entire three-dimensional (3-D) velocity field was calculated at once without assuming any periodicity in the flow field.

The nodal values of velocity and pressure, obtained for each of the 9 geometries at 6 flow conditions, serve as the starting point for mixing analysis by Lagrangian particle tracking calculations. Particle trajectories are computed via a fourth-order, adaptive step-size method along the velocity vector field

$$\frac{dx}{dt} = \bar{v}(x) \tag{1}$$

The fundamental process driving mixing in the laminar regime is the stretching of intermaterial surfaces (Chella and

Table 2. Range of Operating Conditions

Case	Reynolds No.
1	$10\times(10)^{1/3}$
2	$10\times(100)^{1/3}$
3	100
4	$100\times(10)^{1/3}$
5	$100\times(100)^{1/3}$
6	1,000

Ottino, 1985; Muzzio and Swanson, 1991; Beigie et al., 1993; Liu et al., 1994). Mixing processes promote contact between mixture components by stretching the interfacial area available for transport of mass and energy and, correspondingly, by decreasing diffusional distances between various species. The rate of increase in the contact area is measured by the stretching of small vectors attached to fluid particles as they move through the flow, which is computed by integrating Eq. 2

$$\frac{dl}{dt} = (\nabla v)^T \cdot l \quad \text{(with the initial condition } l_{t=0} = l_0\text{)} \quad (2)$$

The accumulated stretching (such as strain) for a given particle trajectory is defined as

$$\lambda = \frac{|l|}{|l_0|} \quad (3)$$

(The accumulated stretching has also been defined as the stretch ratio (Ottino et al., 1979).)

As we will see below, stretching calculations are used in various ways to quantify the efficiency of a mixing process. In increasing the degree of resolution, the arithmetic mean stretching measures the global rate of generation of intermaterial area (that is, global rate of mixing). The spatially resolved stretching field quantifies the intensity of the mixing process as a function of position and time (Muzzio and Swanson, 1991; Ottino et al., 1992). The statistical frequency of λ values computes the spectrum of mixing intensities and, as explained below, it is the key to a rational definition of mixture quality parameters. It is computed as

$$H_n(\log \lambda) = \frac{1}{N} \frac{dN(\log \lambda)}{d \log \lambda} \quad (4)$$

where N is the total number of vectors used to compute the stretching field. Since the rate of accumulation of λ is exponential, the evolution of the stretching in chaotic flows can be best described using a logarithmic scale. The base 10 logarithm of λ is adapted for all results discussed in this article.

Typical computations simulating 10% injection by volume of an additive with equal density and viscosity as the main fluid are performed by injecting a blob of 200,000 computational particles along the centerline of the Kenics. The particle trajectories are computed according to Eq. 1. These computations are validated by comparison to experimental data available in the literature (Pahl and Muschelknautz, 1982). The computational results are treated in the same manner as in the experimental report. The homogeneity of the system is assessed by computing the decrease in the variation coefficient of "sample compositions" (Danckwertz, 1952). The mixer cross-section is divided into a 70×70 grid of equal-size cells. Only the cells that are entirely within the mixer cross-section are retained. The number-based standard deviation σ_N is computed as

$$\sigma_N = \sqrt{\frac{\sum_{i=1}^{\text{ncells}} (N_i - \bar{N})^2}{\text{ncells} - 1}} \quad (5)$$

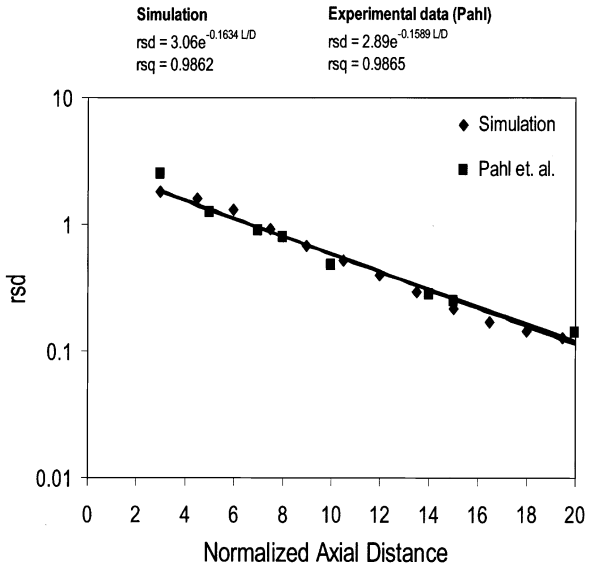

Figure 2. The computed relative standard deviation (rsd) is in excellent agreement with experimental data obtained by Pahl and Muschelknautz (1982) in the standard Kenics mixer at *Re* = 0.15.

where N_i is defined as the number of tracer particles in box i, and $\bar{N}$ is the mean number of particles per cell. Then, the variation coefficient (a.k.a. the relative standard deviation, RSD) at each axial cross-section is computed according to

$$\text{RSD} = \sqrt{\frac{(\sigma_N^2 - \sigma_\infty^2)}{\bar{N}^2}} \quad (6)$$

Here, σ_∞ is the residual value of the number-based standard deviation (a finite value for a certain number of tracer particles), estimated by the value of σ^2 at the end of 24 mixer elements.

Figure 2 compares the decrease in RSD with the number of mixer elements for $Re = 0.15$, where both the simulated and the experimental data are indicated. Following the experimental conditions used by Pahl and co-workers, the RSD in the Kenics was computed for creeping flow conditions. Linear regression of the data is used to compute the mixing rate, which is given by the slope of the RSD curve vs. the number of mixer elements on a log scale. The RSD decreases at an exponential rate over 20 mixer elements with a slope of -0.1634 in the computations, which is within 3% of the experimental slope of -0.1589 (the correlation coefficient R^2 for both the experimental and the computational data is 0.986). Such excellent agreement between the numerical results and the experimental data is representative of the accuracy of the numerical algorithms used for the mixing simulations presented in this article.

In the next section, CFD results are used to examine the effect of design parameters in detail.

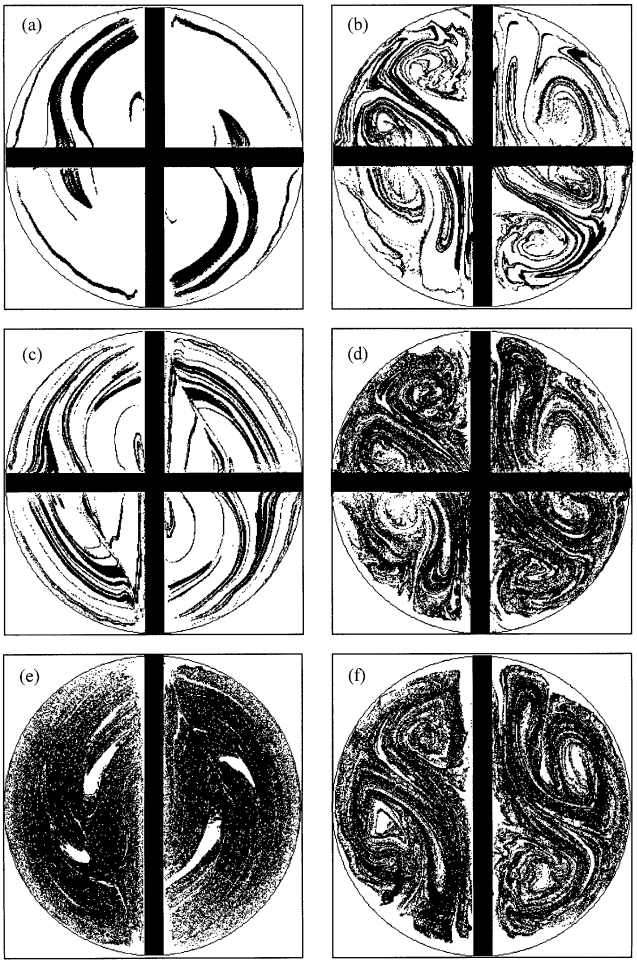

Figure 3. Injecting an equal viscosity additive (10% by volume) just upstream of the inlet region reveals nonuniform mixing in the standard Kenics.

Tracer mixing patterns for $Re = 10(10)^{1/3}$ are shown on the righthand side after (a) 2, (c) 8 and (e) 22 mixer elements. On the lefthand side, mixing patterns at $Re = 1{,}000$ are indicated after (b) 2, (d) 8, and (f) 22 mixer elements.

Mixing Performance of the Standard Kenics Mixer

Mixing simulations are shown in Figure 3. The lefthand side of Figure 3 corresponds to three cross-sectional cuts along the Kenics mixer at $Re = 10(10)^{1/3}$. Inertial effects on the flow at this *Re* are small compared to those observed for $Re = 1{,}000$ (righthand side of the figure). Both cases immediately reveal that the tracer, initially injected at the center of the pipe, does not spread uniformly throughout the flow domain. Quite the contrary, it forms a well-defined pattern consisting of a thousand of nested striations. Moreover, as the mixing process continues, a self-similar process dominates the evolution of the mixture. As the fluid travels through an increasing number of elements, the mixture displaying increasingly finer striations organized in a self-preserving topology.

The evolution of the mixing pattern at $Re = 1{,}000$ is depicted in Figures 3b, 3d and 3f, where the striated mixing pattern is visible even after 22 Kenics elements. Surprisingly, even though the end result of the mixing process at $Re = 1{,}000$ in (f) is substantially different from (e) at $Re\ 10(10)^{1/3}$, it evolves in the same manner. Independently of the amount of inertia, the same fundamental behavior is observed at both the low and high flow regimes, indicating that asymptotic directionality (AD) is a universal property of chaotic mixing processes in static mixers for the full range of *Re* from creeping flow to the brink of turbulence. In the next section we examine the stretching field in the Kenics mixer, which provides further evidence for the existence of self-similar mixing processes in the 3-D mixing system.

Self-similarity of the stretching field

We computed the stretching of small fluid filaments by the methods described earlier (see Eq. 2). The amount of stretching each portion of fluid experiences during the mixing process determines the mixture quality and intensity at each spatial position. Initially, 200,000 passive tracer particles were distributed uniformly in a plane halfway into the first mixer element (that is, $x = 1/2$ L) in each geometry listed in Table 1. We chose this starting position for the particles, because the flow is the same upstream and downstream with respect to this plane in the absence of inertia (Hobbs and Muzzio, 1998a). A stretching vector of initial dimensionless length $|l_0| = 1.0$ was attached to each fluid tracer particle. The initial orientation of each infinitesimal vector was random in the 3-D flow field. The spatial position and the accumulated stretching of each fluid tracer was recorded as the particles passed through 24 mixer elements (that is, after $(2+1/2)$L, $(4+1/2)$L, $(6+1/2)$L, ... $(22+1/2)$L). These downstream distances are equivalent to units of 1 flow period. (The first flow period is indicated in Figure 1 with a schematic drawing of the standard Kenics mixer for further clarification.)

Contours of the accumulated stretching at three axial locations are examined in Figure 4 at two flow rates. The three figures on the lefthand side show the stretching field after 1, 3, and 5 flow periods at $Re = 10(10)^{1/3}$ in Figures 4a, 4c, and 4e. Results on the righthand side of Figures 4b, 4d, and 4f correspond to the same axial locations at a higher flow rate, $Re = 1{,}000$. The accumulated stretching is color-coded on a logarithmic scale according to the total magnitude, and plotted as a function of initial particle positions. In order to highlight the effect of tracer injection positions, regions of low stretching appear in white/gray and regions of high λ are represented by black/dark gray. The cross-section of the mixer elements is represented by the white rectangle along the diameter of the pipe in all the contour plots.

It is immediately apparent that the stretching field in the standard Kenics at low flow rates is highly nonuniform. The magnitude of accumulated stretching at different locations in the flow spans several orders of magnitude. This observation could be important to industrial practitioners, because the distribution of stretching intensities is directly related to the intensity of mixing experienced by material injected in each region of the flow. Furthermore, it determines the amount of intermaterial area available for diffusional transport, thus setting up the landscape of reaction zones in the mixer. Based on such an inhomogeneous field of mixing intensities, significant variations in the local reaction rate and selectivity should be expected in reactive applications; that is, the spatial distribution of stretching can help in practical applications to se-

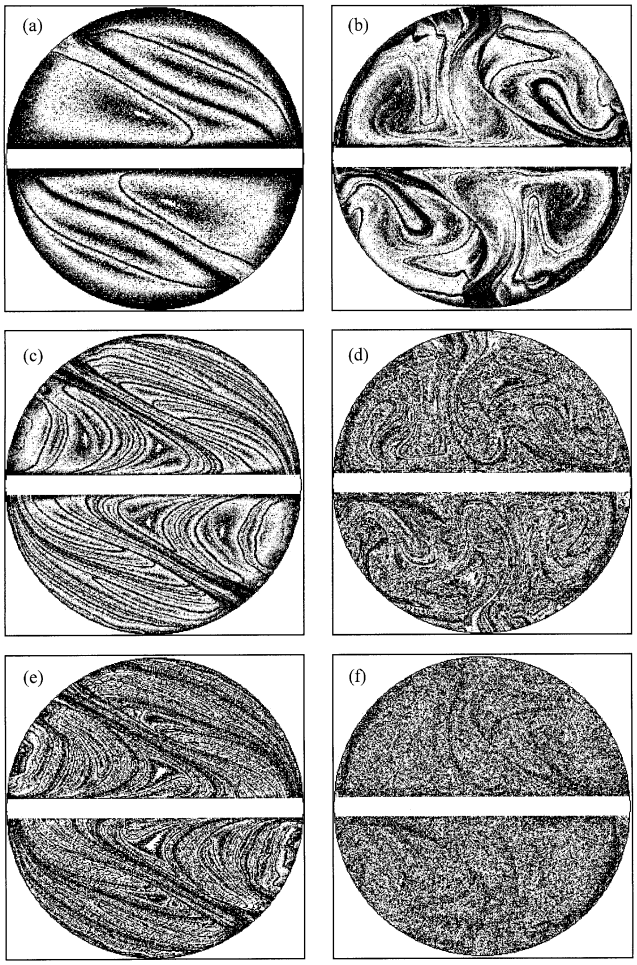

Figure 4. Effect of Reynolds number on mixing performance in the standard Kenics.

Contours of the accumulated stretching ($\log_{10}\lambda$) are shown for $Re = 10(10)^{1/3}$ on the lefthand side, and for $Re = 1{,}000$ on the righthand side at three axial locations: (a)–(b) after 2 elements, (b)–(c) after 6 elements, and (d)–(e) after 10 elements.

lect an efficient injection location for distributing an additive or a reactant. For example, Figure 4 suggests that fluids can be distributed more rapidly and efficiently in the laminar flow regime, if injected along the walls into dark, high-stretching areas in the flow. This is fortuitous since these are also the regions of the flow that allow maximum heat transfer, and, thus, best control of the temperature, which is critical in most reactive applications.

The existence of segregated regions, or islands is indicated by the appearance of coherent low-stretching areas in the flow. At $Re = 10(10)^{1/3}$, several low-stretching regions emerge in the flow above and below the static mixer element centered around elliptic (nonchaotic) "islands". Islands have been previously documented in the Kenics at $Re = 100$ (Hobbs and Muzzio, 1998b). In this article, we show that islands occur for a larger range of flow rates and appear at lower Re numbers than proved earlier. These barriers to mixing become insignificant only when the flow rate is increased by more than one order of magnitude (beyond $Re = 500$). Inertial effects homogenize the mixture faster at $Re = 1{,}000$ than at $10(10)^{1/3}$, and only tiny low-stretching spots are visible after 22 mixer elements.

As the mixing patterns have also demonstrated in Figure 3, the apparent self-similarity in the temporal evolution of the stretching field is due to a property called asymptotic directionality. (Compare Figures 4a, 4c and 4e.) Due to this property, a material line that visits a certain region in the flow adopts an orientation that is characteristic of that position and independent of time. Therefore, periodic snapshots of the cross section at different axial distances look the same qualitatively, with some more local detail added after each period but preserving the global structure. The surprising observation in Figure 4 is the emergence of a self-similar pattern in the stretching field at $Re = 1{,}000$. Small-scale structures dominate the evolution of the topology at this condition, indicating that the flow is close to becoming turbulent. However, the self-similar structure of the stretching field indicates that the mixing behavior of the system is governed by the same phenomena at high values of Re as in the deep laminar regime, and, as a result, a great deal of order is detected in this flow. The overall appearance of the stretching field after five periods is more uniform at $Re = 1{,}000$, but high-stretching manifolds near the solid walls and the center can still be identified.

The self-similar behavior that appears in the stretching contours can be characterized in a more quantitative manner by computing the probability density functions corresponding to each Reynolds number. Equation 4, discussed in the previous section, was used to analyze the stretching statistics at each axial cross-section. Figure 5 indicates the computed pdfs for $Re = 1{,}000$ in the standard Kenics geometry with $L/D =$

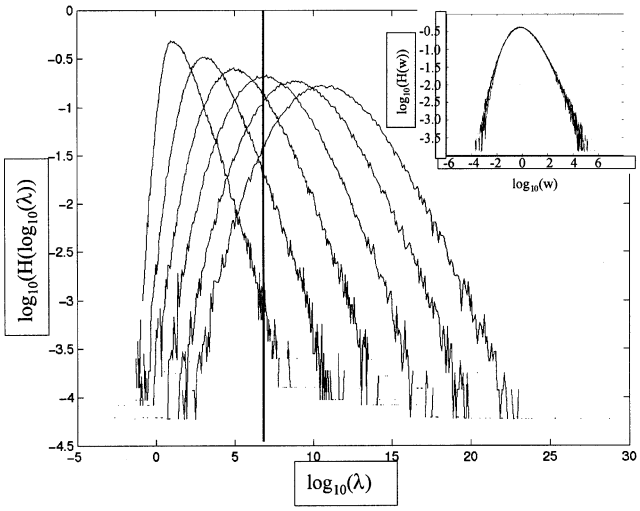

$$w = \log_{10}\lambda - \langle \log_{10}\lambda \rangle / \sigma_{\log(\lambda)}$$

$$H(\log_{10}\lambda) = \sigma_{\log(\lambda)} H(w)$$

Figure 5. Self-similar evolution of stretching at a high flow rate in the standard Kenics at $Re = 1{,}000$.

The probability density function of $\log_{10}(\lambda)$ progressively broadens after 2, 6, 10, 14, 18, and 22 elements. The inset in the figure indicates that all the pdfs can be collapsed onto a single master curve by using standardization.

1.5 and twist per element of 180°, where each curve corresponds to a different axial cross-section along the mixer. After 2, 6, 10, 14, 18, and 22 elements, the stretching distributions broaden and move to the right as the fluid moves downstream in the mixer. The mean stretching increases about five orders of magnitude for each curve, which means that the average diffusional distance (that is, the thickness of each material filament) shrinks at an equal rate. It is also interesting to note that a small fraction of tracer elements have a small accumulated stretching even after passing through 22 mixer elements in the Kenics mixer. It is due to having regions of nonchaotic flow in the device that do not experience exponential stretching. Another indication of this phenomena is the appearance of some small "bumps" on the low stretching side of the distributions, which also suggest that small islands are still present in the flow even at high flow rates. The changing shape of the distribution curve for the first few periods of the flow demonstrates the asymptotic approach to the invariant template. Standardization, a common statistical tool, can be used to reveal the self-similar characteristics of stretching at $Re = 1{,}000$. The mean of $\log_{10}\lambda$ is subtracted from the data and then divided by the standard deviation. We can define a new variable

$$w = \frac{\left(\log_{10}\lambda - \langle \log_{10}\lambda \rangle\right)}{\sigma_{log_{10}\lambda}} \tag{7}$$

and the scaled distributions are then given as $H(w) = dN(w)/dw$. Standardization collapses the distributions of stretching values to a single curve, as displayed in the inset of Figure 5. Here, the scaled curves span over 9 orders of magnitude. Having a broad spectrum of mixing intensities is intrinsic to all chaotic flows. However, the self-similar evolution implies that, once the invariant structure of mixing intensities emerges with enough detail, it can be predicted for any subsequent location in the flow. We can exploit this property of chaotic flows to select the desired mixture quality *a priori* when designing a static mixer for viscous mixing applications.

Effect of Flow Rate and Design Parameters

Residence time distribution (rtd) is the most common specification used in typical equipment design problems. The rtd gives bulk information about the flow in a device, such as whether short-circuiting may occur, or if significant pockets of fluid are segregated from the bulk. On the other hand, it cannot be used to pre-select the final mixture quality. The rtd is not sufficient to characterize mixing microstructure; it does not account for the distribution of intermaterial area, stretching rates and striation thicknesses. These measures are important parameters in determining the intimacy of contact between mixture components.

L/D effects as a function of Reynolds number

The energy cost of inline mixers is measured by the pumping cost of the fluids. Increasing the number of mixer elements or the torsion is counter-balanced by the increase in pressure cost. The energy required to drive the reorientation process generates an increased pressure drop through the same number of elements at lower aspect ratios. Figure 6 illustrates the change in pressure drop per element as the aspect ratio and the flow rate are increased in the Kenics mixer. The twist angle per element was kept constant at 180°. The average pressure at the inlet of the mixer was computed at 1,000 points in the cross-sectional plane, and the same method was used to obtain the pressure at the outlet before computing the pressure drop per element. The three curves in Figure 6 correspond to three flow rates, where the lowest and the highest values of *Re* are the same as in Figures 4a and 4b, $Re = 10(10)^{1/3}$, and $Re = 1{,}000$. Decreasing *L/D* at $Re = 10(10)^{1/3}$ does not increase the pressure drop per element significantly. However, the slope of the top two curves, which represent two higher flow rates, is significantly greater, indicating a stronger dependence on the aspect ratio. In other words, there is a higher energy price associated with the shorter *L/D* designs.

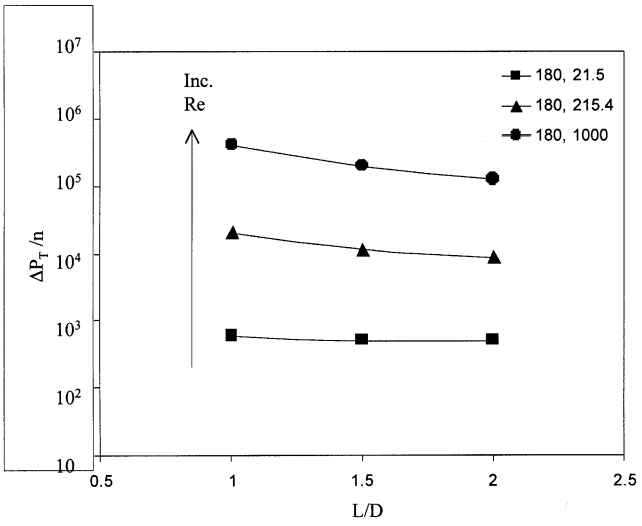

Figure 6. Increasing the aspect ratio (*L/D*) lowers the pressure drop per element in the Kenics.

This inverse relationship is magnified at higher flow rates.

We have demonstrated so far that even though the flow in the standard Kenics mixer is chaotic, it does not produce mixtures with uniform micromixing intensities. The presence of segregated regions (elliptic islands) in the flow further hinders mixing efficiency. Destroying these regular flow regions should be a primary concern in applications. A natural question is whether islands can be minimized by modifications in the standard mixer design. In an effort to test the effects of geometric parameters on mixing performance, we examined the evolution of stretching in each of the 9 geometries listed in Table 1 at the flow rates given in Table 2. Hereon, we refer to particular mixer geometries with the number assigned in the lefthand side column of Table 1.

Figure 7 compares the stretching intensities in geometries 3, 6, and 9, where the twist angle per element is kept constant at 180°, but *L/D* is varied from 1 to 2. Consider the contours of $\log_{10}\lambda$ for the three mixer geometries, where the righthand side of the figure represents $Re = 10(10)^{1/3}$ and the lefthand side corresponds to $Re = 1{,}000$. As before, the mixer housing appears as a circle and the white rectangle in the

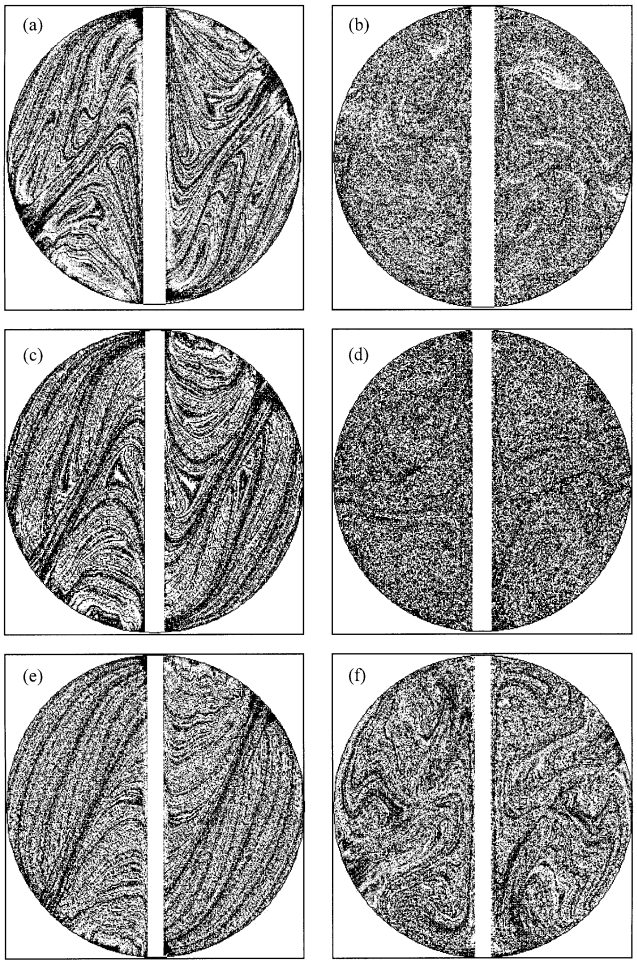

Figure 7. Contours of $\log_{10}\lambda$ also reveal that the aspect ratio has noticeable effects on mixing performance.

The lefthand column in the figure represents contours of $\log_{10}\lambda$ at $Re = 10(10)^{1/3}$, and the righthand side corresponds to $Re = 100(10)^{1/3}$ for (a)–(b) $L/D = 1$, (c)–(d) $L/D = 1.5$, and (e)–(f) $L/D = 2$.

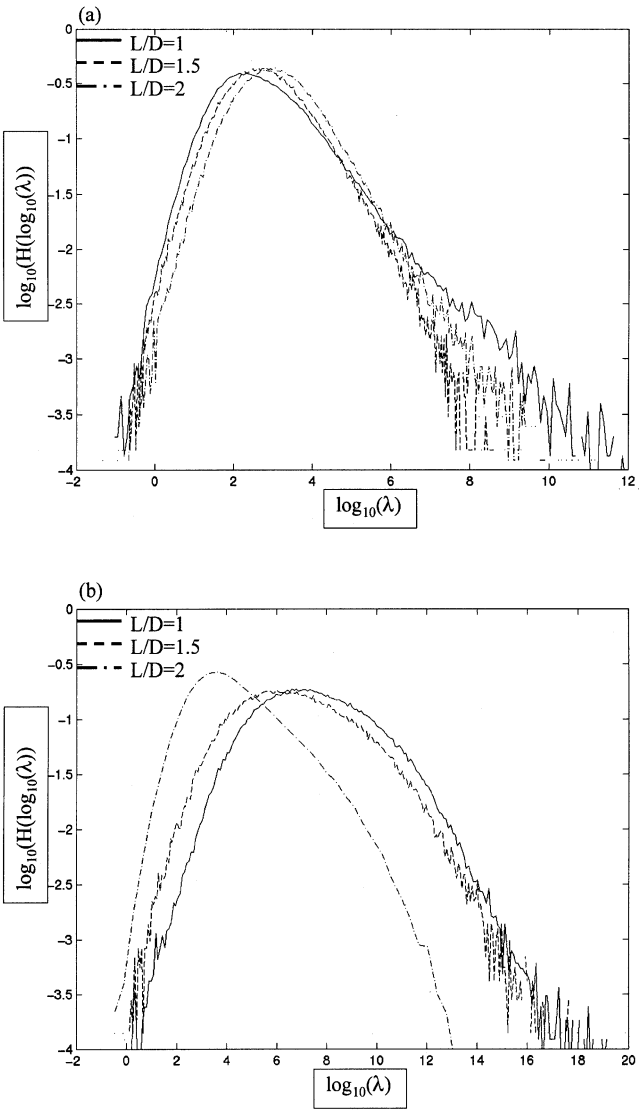

Figure 8. Pdf of $\log_{10}\lambda$ at three aspect ratios (L/D) in the Kenics mixer.

If the twist angle is constant at 180°, differences are noticeable mainly at the high-stretching side at lower flow rates: (a) at $Re = 10(10)^{1/3}$; (b) the effect of L/D on mixing performance becomes pronounced as inertial effects increase at $Re = 1{,}000$.

figure is the cross-sectional view of the static mixer element. The top two contours in Figures 7a–7b represent an axial distance of (10 + 1/2)L in geometry 3, where the aspect ratio of each element (L/D) is 1. This is the lowest aspect ratio examined in this article. Figures 7c–7d and 7e–7f correspond to $L/D = 1.5$ and $L/D = 2$ at the same flow rate and axial distance, respectively. At $Re = 10(10)^{1/3}$, the effect of L/D on the stretching field is minor. The structure of high stretching manifolds is largely unchanged, and large segregated regions appear for all three values of the element aspect ratio. As L/D is increased from 1 to 1.5 and 2.0 (Figures 7a, 7c and 7e), while the size of the islands decreases and their shape and location changes, slow mixing regions (white/light gray colored areas) are apparent in all three geometries.

Mixing intensities appear to be more spatially homogeneous at $Re = 1{,}000$ for the two geometries with smaller aspect ratios. In Figure 7d, there are no large low-stretching regions in the cross-sectional area and only minor low stretching regions are observed in Figure 7b. On the other hand, at $L/D = 2$, larger coherent segregated regions are apparent. As the flow rate is gradually increased, islands of various sizes remain in the flow. At $Re = 1{,}000$, the stretching field is still less homogeneous at $L/D = 2$ (Figure 7e), than for the lower aspect ratios.

The influence of the element aspect ratio L/D on mixing performance is immediately apparent in the stretching probability distributions. Figure 8a represents the pdf($\log_{10}\lambda$) after 10 mixer elements for $Re = 10(10)^{1/3}$, whereas Figure 8b indicates the pdf($\log_{10}\lambda$) at $Re = 1{,}000$. In both cases, the twist angle is kept constant at 180°. The two distributions corresponding to the two larger L/D values appear to have identical shapes. However, the pdf($\log_{10}\lambda$) has a distinct tail at $L/D = 1.0$, indicating strongly coherent high stretching areas

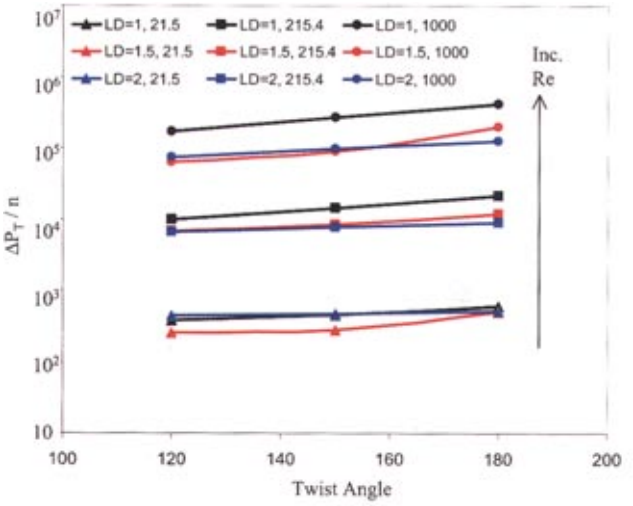

Figure 9. Increasing the twist angle also increases the pressure drop per element, due to a greater pitch of the mixer elements.

in the flow. The situation is quite different for $Re = 1{,}000$, where the $L/D = 2$ flow produces significantly less stretching after the same number of mixer elements than the other two cases. The other two distributions are more symmetric, closer to a log-normal distribution in shape, indicating that the flows for $L/D = 1$ and 1.5 create a more uniform field of mixing intensities. The inverse relationship of element aspect ratio and mixing performance is due to more frequent reorientations of the flow at lower values of L/D. The rate of stretching depends significantly on the cutting and folding process occurring at the element-to-element transitions. In fact, at low Re, the flow would not be chaotic without these regions. As the L/D ratio decreases, the fluid encounters these regions more frequently as it travels downstream.

Increasing the twist angle per element as a means of gaining improvements in mixing performance also results in significant effects on the pressure drop through the device. Recall that the pressure drop across an element is the driving force for flow through each element of a static mixer, representing the energy cost for the flow. The pressure drop per element differs significantly as the twist angle of each element is altered. Figure 9 includes pressure drop data for all 9 geometries considered in this study. It is apparent that the curves have a positive slope for each of the three flow rates shown in the figure. Thus, there is a tendency of increasing $\Delta P_T/n$ as the twist angle is increased, which is exactly the opposite trend than observed for changes in the aspect ratio.

Twist effects as a function of Reynolds number

Next, we consider the effect of changing the twist angle in order to improve mixing efficiency. Figures 10a–10f reveal the contours of the accumulated stretching in the Kenics mixer at $Re = 10(10)^{1/3}$ and $Re = 1{,}000$. Each of the six plots represents the same axial distance along the mixer, after the fluid passed through a total of 10 elements. The rotation of the 10th element pictured here is from left to right (or clockwise), so the three twist angles in increasing order can be

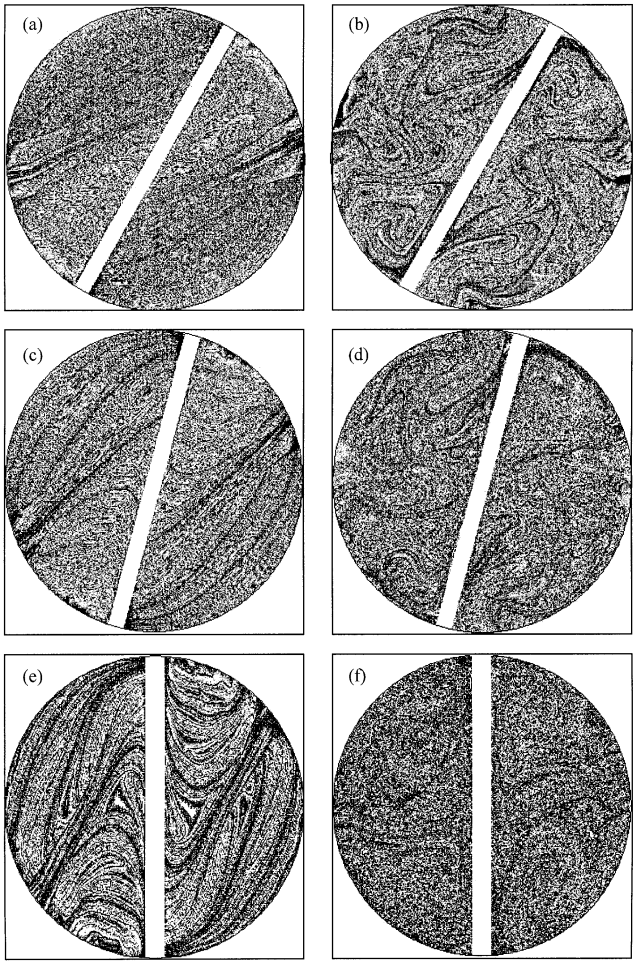

Figure 10. Twist angle significantly affects mixing performance in the Kenics.

Contours of $\log_{10}\lambda$ after 10 mixer elements at two flow rates: (a)–(b) twist angle of 120°, (c)–(d) 150°, and (e)–(f) 180° at $Re = 100$ and $Re = 100(10)^{1/3}$, respectively. The aspect ratio, L/D is kept constant at 1.5 for all cases considered here.

easily distinguished in the three rows of Figure 10. Figures 10a–10b represent 120° twist per element, Figures 10c–10d are for 150°, and Figures 10e–10f are for 180°, where the aspect ratio was kept constant at 1.5 for all six contours presented here. (These geometries are 4, 5, and 6 in Table 1.) At the lower Re, there is a clear decrease in mixing performance as the twist angle is increased. The case with 120° twist appears to be most homogeneous, followed by 150° and 180°. Mixing appears to improve with increasing twist angle for $Re = 1{,}000$. Next, we examine the pdf($\log_{10}\lambda$) for each of these three geometries in Figure 11. The first part of the figure (Figure 11a) corresponds to $Re = 10(10)^{1/3}$ and the second part is $Re = 1{,}000$ (Figure 11b). The slowest rate of stretching corresponding to the 180° geometry at low Re is apparent in Figure 11a. This flow contains macroscopic islands (as opposed to the other two cases, see Figure 10e), so it is not surprising that the stretching accumulates more slowly. This is a clear indication that the mixing performance of this configuration is less effective after the same number of Kenics

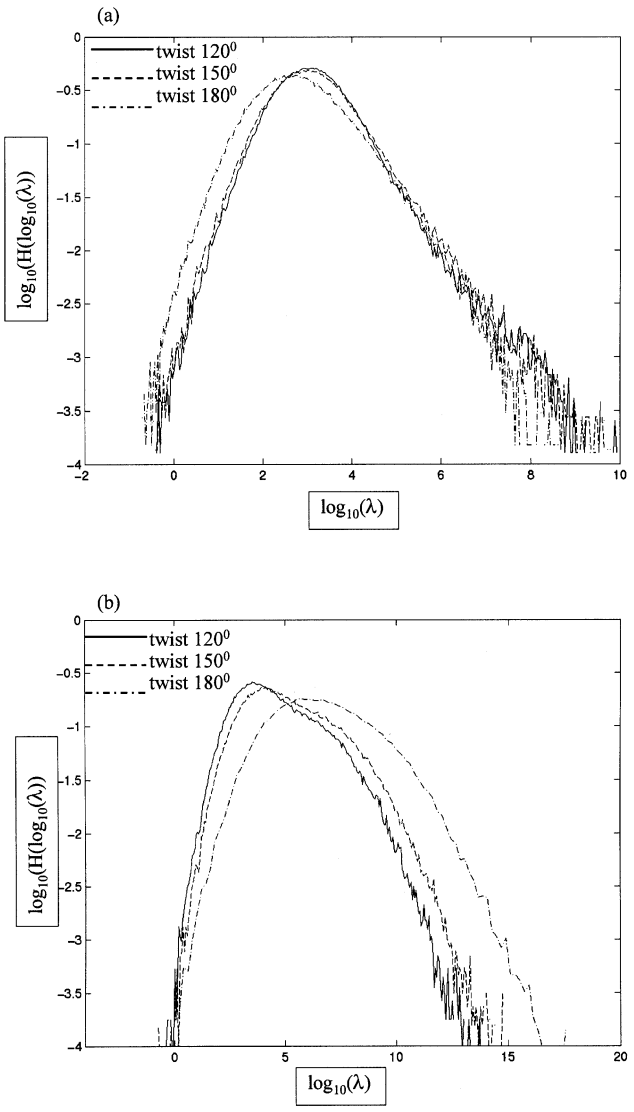

Figure 11. Pdf($\log_{10}\lambda$) at three twist angles in the Kenics mixer.

The aspect ratio is kept constant at $L/D = 1.5$. For $Re = 10(10)^{1/3}$ in (a), the mean stretching rate is distinctly lower in the standard geometry. For $Re = 1{,}000$ in (b), as inertial effects increase, the trend reverses.

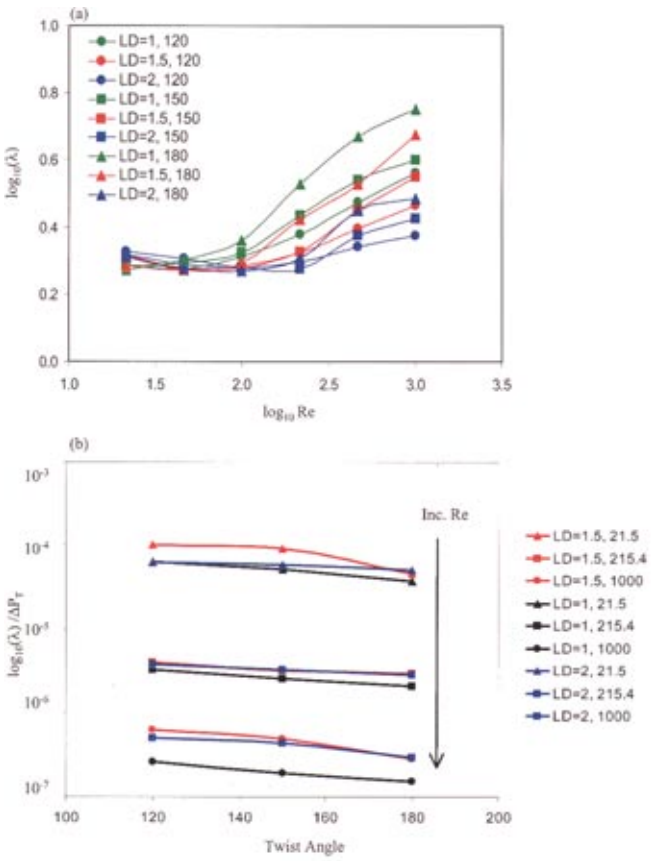

Figure 12. Average accumulated stretching can be used to determine mixer efficiency during equipment design.

In (a) $\log_{10}\langle\lambda\rangle$ is plotted for all 9 variations considered, as a function of the Reynolds number. In (b) $\log_{10}\langle\lambda\rangle/\Delta P$ decreases for low and higher flow rates in the Kenics, indicating that significant gains in mixing performance can be accomplished by decreasing the twist angle per element.

elements. The trend is reversed for $Re = 1{,}000$, where the geometry with 180° elements appears to have the largest mean stretching (Figure 11b). This configuration creates the most uniform spectrum of mixing intensities and distributes materials most homogeneously at high Re.

Up to this point, we considered the effect of both the element aspect ratio and the twist angle on stretching. Universal trends for mixing performance could not be established. Inhomogeneities of various degrees were noticeable at different positions in each geometry depending on the flow rate, indicating that there is no *a priori* method to predict the mixing behavior as a function of twist angle at various flow rates. One common trend in behavior among the three geometries is that mixing is not improved with increasing flow rate. The most homogeneous conditions seem to exist at the lowest flow rate for 120° and 150°, and large size islands appear in the standard geometry until $Re = 100(10)^{1/3}$.

The observed mixing behavior can be compared for different configurations by computing $\log_{10}\langle\lambda\rangle$, which is proportional to the average mixing rate in a chaotic flow. Figure 12a summarizes that data for all 54 cases considered. The aspect ratios are represented by three different colors and the twist angles are distinguished by different symbols to facilitate comparison that is, the green curves show data for $L/D = 1$, the red curves stand for $L/D = 1.5$, and the blue curves represent $L/D = 2$. Circles are used for all 120° twist, squares for all 150° twist, and triangles for all 180° twist. Some characteristics are common for all 54 cases considered. There is a flat region in the curves at lower Re numbers that rises sharply near $Re = 100$. The minimal dependence of $\log_{10}\langle\lambda\rangle$ on Re at lower Re is another indication that L/D is not very important for flows with low inertia. On the other hand, there is a distinct difference in $\log_{10}\langle\lambda\rangle$ for the higher Re regime, indicating a significant effect of L/D on mixing behavior exists at higher flow rates (above $Re = 100$). Consider the set of green curves representing $L/D = 1.0$. If the aspect ratio is kept constant, the mixer with 180° elements performs best according

to the values of $\log_{10}\langle\lambda\rangle$. These features are not unique to this aspect ratio, but also hold true for $L/D = 1.5$ (red curves) and $L/D = 2$ (blue curves). Without accounting for the difference in the driving force required for each flow, Figure 12a suggests that the design with the lowest aspect ratio and highest twist angle is most effective.

Next, we take into account energy cost by normalizing the mixing efficiencies in Figure 12a by ΔP, where ΔP represents the per element pressure drop. The normalized mixing efficiency, $\log_{10}\langle\lambda\rangle/\Delta P$ in Figure 12b provides an equal basis for comparison. Again, three colors are used to differentiate the three L/D ratios, and three different symbols represent the twist angles. The three groups of curves show data for three different flow rates. All curves have a decreasing slope as the twist angle of the mixer elements is increased, indicating a reverse correlation between the mixing performance and the twist angle. This finding is surprising in light of the previous results of Figure 12a. The trend in mixing behavior is now the opposite, showing that the efficiency actually decreases with increasing twist angle.

An even more nonintuitive observation is that the mixing per energy input is not necessarily the highest for higher *Re* flows in the laminar regime. The normalized efficiency $\log_{10}\langle\lambda\rangle/\Delta P$ is much higher for low *Re* flows than it is for high *Re*. Compare the three curves in the top part of the graph (plotted with triangles), where $Re = 10(10)^{1/3}$, and the three bottom curves (plotted with circles), where $Re = 1{,}000$. There is about a twofold increase in efficiency between the highest and lowest Reynolds numbers. The third set of data (plotted with squares) represents $Re = 100(10)^{1/3}$, which is an intermediate flow rate. It falls between the low and high extreme on the efficiency plot, as expected. When trying to mix highly-viscous and shear-sensitive materials, greater mixing action can be achieved at a lower flow rate in the Kenics mixer than at near turbulent conditions.

While performance characterization based on the average behavior such as those described above can be useful, in particular in view of the fact that, due to AD, the system is characterized by a single global mixing rate, one can easily envision the need to develop other methods that account for the variability in the local intensity of the mixing process. In the next section, we use self-similarity criteria to develop such a measure of performance.

Microstructure-Based Design of Mixing Devices

Consider an application where the mixing requirement is to have all fluid striations smaller than a given size specification. One might want to ensure, for example, that the worst-mixed region ensures a certain minimum; this is often a requirement when mixing pigments into plastics. Such a final process requirement can also occur in a polymerization process, where the material properties are determined by the layering and size of the filaments. Another example would be the mixing of immiscible fluids where the striation thickness translates into drops of a particular size. Such a micromixing task can be accomplished if the spatial distribution of stretching is taken into account during equipment design. The necessary link between the size of fluid striations (that is, micromixing quality) and the convective mixing process is provided by stretching, that is, $\lambda \sim \rho \sim 1/s$. An upper limit on the thickness of the striations in a mixture sets a lower limit on the stretching that the fluid must experience during the mixing process. The stretching data in Figure 5 can then be used to ensure a given static mixer configuration can accomplish such a mixing task.

However, since stretching has a continuous monotonic spectrum (and so do striation thicknesses), a more realistic criterion is to define χ as the fraction of all stretching values that exceed a particular value, so that a certain fraction of striations have a thickness under a certain desired value. This can be obtained simply by recalling that

$$\int_0^{\bar{s}} \bar{s}F(\bar{s})\,d\bar{s} = \int_{-\infty}^{\log \bar{s}} \bar{s}H(\log \bar{s})\,d\log \bar{s}$$

$$= \int_{\log \bar{\lambda}}^{\infty} \bar{\lambda}^{-1}\bar{\lambda}H(\log \bar{\lambda})\,d\log \bar{\lambda} = \int_{\log \bar{\lambda}}^{\infty} H(\log \bar{\lambda})\,d\log \bar{\lambda} \tag{8}$$

Thus, a choice of maximum striation value can be used to specify a minimum value of stretching during equipment design based on the process requirements. Thus, if we integrate the area under the stretching spectrum for values larger than a minimum set point (Figure 5), χ spans a range of 0 to 1.0, increasing as we move from the right to the left towards the origin. Figure 13 summarizes the dependence of stretching on the number of mixer elements at $Re = 1{,}000$. The sharp maximum on the left in all the distributions occurs because a very small fraction of fluid elements have very large stretching values.

As we move to the right along the horizontal axis, the fraction of striations in the population increases. Since all striations experience some amount of stretching and deformation in a mixing flow, as the fraction approaches 1.0 on the right, stretching drops asymptotically to 0.0. At $\chi = 0.9$ (marked by a dark line on the figure), the total accumulated stretching exceeded by 90% of the total population can be examined. Recall that 2 Kenics elements correspond to 1 flow period. After 6 elements ($n = 3$), 90% of the striations have stretchings greater than $10^{2.33}$. This means that the striation thickness for 90% of the fluid is $1/10^{2.33} = 0.00468$. As the fluid flows downstream through 18 mixer elements ($n = 9$), the same fraction of striations have a stretching of $10^{6.71}$ or s equal to $1/10^{6.71} = 1.95(10)^{-7}$. In other words, 90% of the fluid is homogeneous below molecular scales.

Since the stretching process in chaotic flows is self-similar, the distributions of $\log_{10}\langle\lambda_\chi\rangle$ also evolve along a self-similar template. Once we normalize the distributions by n, the curves approach an invariant shape as the flow period increases. Thus, it is sufficient to consider the mixing process after 14 Kenics elements. The distribution of striation thicknesses does not change any longer beyond this point. This does not mean that the size of the striations remains constant. It indicates that, except for the effect of diffusion (which will be addressed in future publications), the size of striations changes at the same rate locally after 14 elements as it does after 16, 18, or any point in the device thereafter. In other words, the local mixing intensity reaches a constant and the size ratio of striations in neighboring regions becomes invariant.

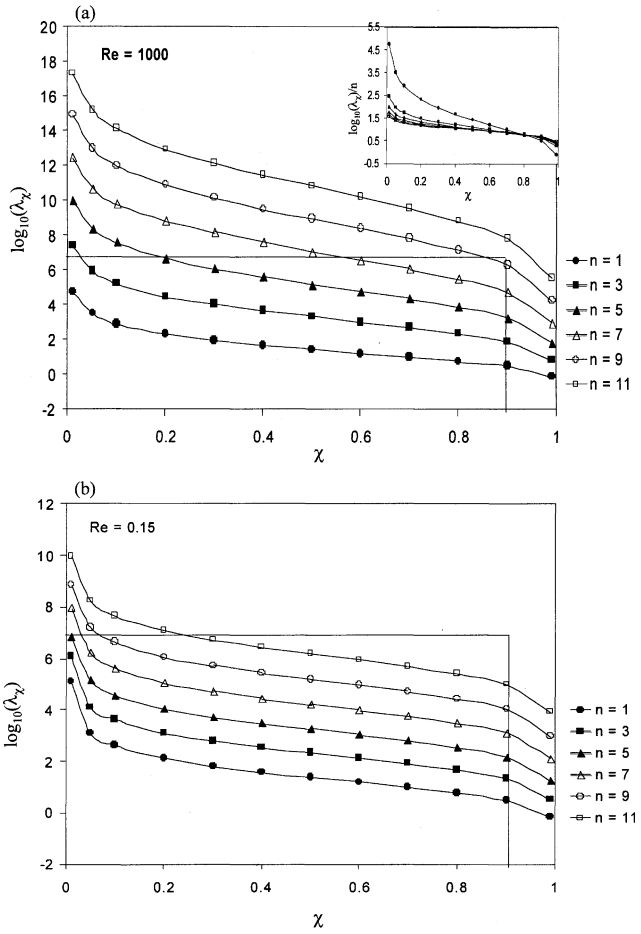

Figure 13. Spatial distribution of stretching and mixing intensity can be taken into account, if a mixing criterion based on the striation thickness distribution is chosen.

In (a) the mixing criterion based on striation thickness is plotted for $Re = 10^3\sqrt{10}$ as a function of the stretching necessary to achieve the required micromixing efficiency. The efficiency curves are plotted for the mixing process at six different mixer lengths: after 2, 6, 10, 14, 18, and 22 Kenics elements. The inset indicates that the efficiency curves collapse to a single curve as the number of flow periods is increased. The same efficiency curves are indicated in (b) for $Re = 1{,}000$.

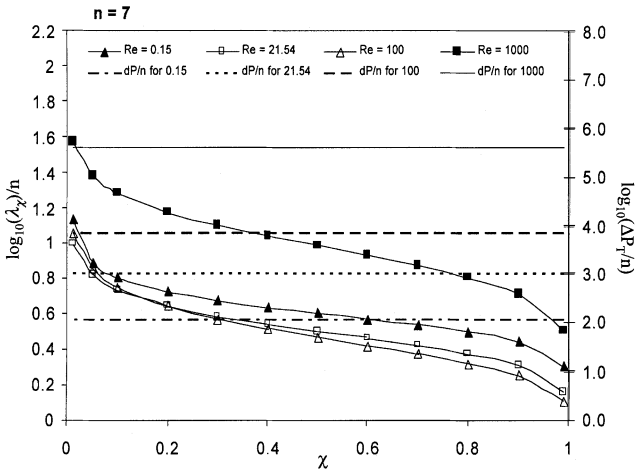

Figure 14. Mixing criterion based on striation thickness is plotted for four different flow rates in the Kenics mixer.

The axis on the lefthand side indicates the necessary stretching for the required striation thickness normalized by the flow period. The axis on the righthand side indicates the pressure drop normalized by the flow period for the four flow rates.

Next, we examine the effect of Re on $\log_{10}\langle \lambda_\chi \rangle$. This helps understand the effect of flow rate on mixture quality. As shown in Figure 13b, for lower Reynolds numbers, the amount of stretching per element is much lower than for the nearly turbulent conditions of Figure 13a, although once again, curves corresponding to different numbers of periods asymptotically approach an invariant shape. Figure 14 describes the asymptotic distribution of $\log_{10}\langle \lambda_\chi \rangle/n$ at different flow rates. The four curves are similar in shape and represent a change in flow rate over four orders of magnitude (from 0.15 to 1,000). Interestingly, the order of the four curves does not follow a monotonic pattern as the Reynolds number increases. The two most efficient Re for decreasing the striation thicknesses in the mixture are $Re = 1{,}000$ (curve with dark squares), followed by $Re = 0.15$ (curve with dark triangles).

The total pressure drop, normalized by the flow period n is also shown on Figure 14 in order to compare the mixture quality *and* the energy cost of the mixing process at each flow rate. Since the operating cost of static mixers is given by the pressure drop required to drive the flow, $\Delta P_T/n$ is the normalized energy cost required to accomplish each flow rate. Let's now demonstrate how this data can be used in a practical design application of a static mixer, where the final mixture quality is chosen as the main criterion.

As an example, consider a mixing process where the required final mixture must have 90% of striations below one-tenth of a micron (that is, $s_{90} < 10^{-7}$ and $\chi = 0.90$ and $\log_{10}(\lambda_{90}) = 7.0$). The fluid viscosity and density (μ and ρ, respectively) are known parameters, and one can obtain a range of standard sizes for the diameter of the mixer housing. The diameter of the static mixer D, the total number of elements ($2n$), and the total pressure drop ΔP_T must be determined for each design. Let us consider a mixer housing with $D = 2.0$ in. $= 5.08$ cm.

Since Figure 13 established that striation thicknesses were reduced most effectively at $Re = 1{,}000$ and $Re = 0.15$, we compare two designs with $Re = 1{,}000$ and $Re = 0.15$. The flow rate for a given D and Re is given by $Q = \Pi D\mu(Re)/4\rho$ and the element length of the mixer is then set by knowing the aspect ratio L/D.

Next, we determine the total number of elements needed for the mixing application, which also establishes the total length of the device. Go to Figure 5, where the required quality ($\log_{10}(\lambda_{90}) = 7.0$) is indicated by a vertical line. At $\chi = 0.90$, we get in Figure 13a approximately $n = 9$. Thus, for 90% of all fluid striations to be thinner than a micron, a total number of 9 flow periods or 18 Kenics elements are required. For the same mixture quality, Figure 13b indicates that approximately 15 flow periods, or 30 mixer elements, are necessary to accomplish the same task at $Re = 0.15$. The 1.5-fold

increase in total length may not be beneficial, for example, if floor space is restricted. However, we now take into account the energy cost of mixing for each design and use Figure 14 to determine ΔP_T for the two designs. For $\chi = 0.90$, $\log_{10}(\Delta P_T) = 5.60$ at $Re = 1{,}000$ (solid dark line) or $\Delta P_T = 3.58(10)^6$ Pa. On the other hand, $\log_{10}(\Delta P_T) = 2.08$ for $Re = 0.15$ (dash-dot line) or $\Delta P_T = 1{,}803$ Pa. There is about a 2,000-fold difference in pumping costs between the two designs. In practice, one can then decide whether the operating costs outweigh the advantage of having a shorter static mixer for a given application.

Conclusions

The Kenics static mixer is the subject of a detailed computational analysis of flow and mixing that includes nine variations in geometry (including the standard design) and six flow conditions. A trend in mixing behavior, previously observed under creeping flow conditions, is reinforced: the element aspect ratio (L/D) does not contribute significantly to mixing efficiency, if the flow is in the low inertia regime (that is, $Re < 100$). However, L/D impacts mixing performance at high flow rates, and promotes the existence of segregated regions in the flow if increased. The mixing efficiency can be affected more significantly by the twist angle per mixer element, which changes performance at both low and high flow rates. We observed a common trend in that the intensity of mixing did not improve monotonically as the flow rate was increased. Segregated zones appeared in the flow at intermediate Re values, and affected a significant range of flow conditions. Taking into account the energy requirements for flow in each design, the mixing efficiency showed a surprising reverse trend with increasing flow rate. Mixing performance was actually greater for flows with a small amount of inertia, than at the near-turbulent condition of $Re = 1{,}000$, which has implications on processes using shear-sensitive viscous materials. The same mixing action can actually be accomplished when lowering the flow rate, sparing the possibility of shear damage to the fluid. Designs with lower twist angles (in the window of 120° to 150°) per mixer element are recommended.

For the first time, we observed that mixing structures evolve along a self-similar template for flows that are approaching turbulence, which implies that the system retains structure and even if inertial forces have a significant contribution to the flow. The characteristic mixing behavior of the system, based on the evolution of the stretching field, is established after about 10 mixer elements, leading to the development of micromixing-based criteria for mixing performance. The range of mixing intensities created by the flow converges to an invariant distribution for all the flow rates considered, which remain highly inhomogeneous throughout the device, regardless of the number of elements added thereafter.

Literature Cited

Alvarez, M. M., and F. J. Muzzio, "The Mechanism of Mixing and Creation of Structure in Laminar Stirred Tanks," *AIChE J.*, (2002).

Avalosse, Th., and M. J. Crochet, "Finite-Element Simulation of Mixing: 2. Three-Dimensional Flow through a Kenics Mixer," *AIChE J.*, **43**(3), 588 (1997).

Bakker, A., "Flow and Mixing with Kenics Static Mixers," *Cray Channels*, **15**(3), 25 (1993).

Beigie, D., A. Leonard, and S. Wiggins, "Statistical Relaxation under Nonturbulent Chaotic Flows: Non-Gaussian High Stretch Tails of Finite-Time Lyapunov Exponent Distributions," *Phys. Rev. Lett.*, **70**(3), 275 (1993).

Cavatorta, O. N., and U. Bohm, "Fluid-Dynamic and Mass Transfer Behavior of Static Mixers and Regular Packings," *AIChE J.*, **45**(5), 938 (1999).

Chella, R., and J. M. Ottino, "Stretching in Some Classes of Fluid Motions and Asymptotic Mixing Efficiencies as a Measure of Flow Classification," *Arch. Rat. Mech.*, **90**, 15 (1985).

Chisti, Y., and M. Moo-Young, "Bioprocess Intensification through Bioreactor Engineering," *T.I. Chem. Eng.-Lond.*, **74** (Part A), 575 (1996).

Danckwertz, P. V., "The Definition and Measurement of Some Characteristics of Mixtures," *Appl. Sci. Res.*, **3**, 279 (1952).

Del Carmen Rey, M., P. Glasserman, and U. Bohm, "Mass Transfer to Regular Packings at Low Reynolds Numbers and under Natural Convection," *Int. J. Heat Mass Transfer*, **41**(12), 1693 (1998).

Giona, M., A. Adrover, F. J. Muzzio, S. Cerbelli, and M. M. Alvarez, "The Geometry of Mixing in Time-Periodic Chaotic Flows. I. Asymptotic Directionality in Physically Realizable Flows and Global Invariant Properties," *Physica D*, **132**, 298 (1999).

Grace, C. D., "Static Mixing and Heat Transfer," *Chem. Proc. Eng.*, **57** (1971).

Hobbs, D. M., and F. J. Muzzio, "Optimization of a Static Mixer Using Dynamical Systems Techniques," *Chem. Eng. Sci.*, **53**(18), 3199 (1998a).

Hobbs, D. M. and F. J. Muzzio, "Reynolds Number Effects on Laminar Mixing in the Kenics Static Mixer," *Chem. Eng. J.*, **70**(2), 93 (1998b).

Hobbs, D. M., P. D. Swanson, and F. J. Muzzio, "Numerical Characterization of Low Reynolds Number Flow in the Kenics Static Mixer," *Chem. Eng. Sci.*, **52**, 1 (1997).

Ishikawa, T., and T. Kamiya, "Limits of Reynolds Number for Effective Use of Heat-Transfer Promoters—Twisted Tape and Static Mixer," *Heat Transfer-Japan. Res.*, **23**(2), 185 (1994).

Jaffer, S. A., and P. E. Wood, "Quantification of Laminar Mixing in the Kenics Static Mixer: An Experimental Study," *Can. J. Chem. Eng.*, **76** (June), 516 (1998).

Kemblowski, Z., and P. Pustelnik, "Residence Time Distribution of a Power-Law Fluid in Kenics Static Mixers," *Chem. Eng. Sci.*, **43**(3), 473 (1988).

Kusch, H. A., and J. M. Ottino, "Experiments on Mixing in Continuous Chaotic Flows," *J. Fluid Mech.*, **236**, 319 (1992).

Lang, E., P. Drtina, F. Streiff, and M. Fleischli, "Numerical Simulation of the Fluid Flow and the Mixing Process in a Static Mixer," *Int. J. Heat Mass Transf.*, **38**(12), 2239 (1995).

Li, H. Z., Ch. Fasol, and L. Choplin, "Hydrodynamics and Heat Transfer of Rheologically Complex Fluids in a Sulzer Smx Static Mixer," *Chem. Eng. Sci.*, **51**(10), 1947 (1996).

Ling, F. H., and X. Zhang, "A Numerical Study on Mixing in the Kenics Static Mixer," *Chem. Eng. Comm.*, **136**, 119 (1995).

Liu, M., R. I. Peskin, F. J. Muzzio, and C. W. Leong, "Structure of the Stretching Field in Chaotic Cavity Flows," *AIChE J.*, **40**(8), 1273 (1994).

Metcalfe, G., C. R. Bina, and J. M. Ottino, "Kinematic Considerations for Mantle Mixing," *Geophys. Res. Lett.*, **22**(7), 743 (1995).

Morris, W. D., and J. Benyon, "Turbulent Mass Transfer in the Kenics Static Mixer," *Ind. Eng. Chem. Proc. Des. Dev.*, **15**(2), 338 (1976).

Muzzio, F. J., M. M. Alvarez, S. Cerballi, M. Giona, and A. Adrover, "The Intermaterial Area Density Generated by Time- and Spatially Periodic 2d Chaotic Flows," *Chem. Eng. Sci.*, **55**, 1497 (2000).

Muzzio, F. J., and P. D. Swanson, "The Statistics of Stretching and Stirring in Chaotic Flows," *Phys. Fluids*, **3**(5), 822 (1991).

Naumann, E. B., "Enhancement of Heat Transfer and Thermal Homogeneity with Motionless Mixers," *AIChE J.*, **25**(2), 246 (1979).

Naumann, E. B., "On Residence Time and Trajectory Calculations in Motionless Mixers," *Chem. Eng. J.*, **47**, 141 (1991).

Nigam, K. D. P., and E. B. Naumann, "Residence Time Distributions of Power-Law Fluids in Motionless Mixtures," *Can. J. Chem. Eng.*, **63**, 519 (1985).

Ottino, J. M., W. E. Ranz, and C. W. Macosko, "A Lamellar Model for Analysis of Liquid-Liquid Mixing," *Chem. Eng. Sci.*, **34**, 877 (1979).

Ottino, J. M., F. J. Muzzio, M. Tjahjadi, J. G. Franjione, S. C. Jana, and H. A. Kusch, "Chaos, Symmetry and Self-Similarity: Exploiting Order and Disorder in Mixing Processes," *Science*, **257**, 754 (1992).

Pahl, H. M., and E. Muschelknautz, "Static Mixers and Their Applications," *Int. Chem. Eng.*, **22**(2), 197 (1982).

Pustelnik, P., "Investigation of Residence Time Distribution in Kenics Static Mixers," *Chem. Eng. Proc.*, **102**, 147 (1986).

Rauline, D., J. M. Le Blevec, J. Bousquet, and P. A. Tanguy, "A Comparative Assessment of the Performance of the Kenics and Smx Static Mixers," *Trans I Chem. E.* (Part A), 389 (2000).

Rauline, D., P. A. Tanguy, J. M. Le Blevec, and J. Bousquet, "Numerical Investigation of the Performance of Several Static Mixers," *Can. Can. J. Chem. Eng.*, **76**, 527 (1998).

Taweel, A. M., and C. Chen, "A Novel Static Mixer for the Effective Dispersion of Immiscible Liquids," *T. I. Chem. Eng. Lond.*, **74** (Part A), 445 (1996).

van der Meer, Th. H., and L. Hoogedoorn, "Heat Transfer Coefficients for Viscous Fluids in a Static Mixer," *Chem. Eng. Sci.*, **33**, 1277 (1978).

Wang, K. B., and L. T. Fan, "Mass Transfer in Bubble Columns Packed with Motionless Mixers," *Chem. Eng. Sci.*, **33**, 945 (1978).

Zalc, J. M., E. S. Szalai, M. M. Alvarez, and F. J. Muzzio, "Using CFD to Understand Chaotic Mixing in Laminar Stirred Tanks," *AIChE J.*, **48**(10), 2124 (2002).

Zalc, J. M., M. M. Alvarez, and F. J. Muzzio, "Simulation of Flow and Mixing in Stirred Tank Reactors," *ASME Int.*, **397**(2), 233 (1999).

Zalc, J. M., E. S. Szalai, S. Jaffer, and F. J. Muzzio, "Characterization of Flow and Mixing in the SMX Static Mixer," *AIChE J.*, **48**(3), 427 (2001).

Manuscript received Mar. 25, 2002, revision received Apr. 3, 2003, and final revision received Jun. 18, 2003.